Dichroic Thin Films of Silver Nanoparticle Chain Arrays on Facetted Alumina Templates

ARTICLE *in* NANO LETTERS · DECEMBER 2002

Impact Factor: 13.59 · DOI: 10.1021/nl025808r

3 AUTHORS, INCLUDING:

Emmanuel Fort
MINES ParisTech
89 PUBLICATIONS **1,373** CITATIONS
SEE PROFILE

Christian Ricolleau
Paris Diderot University
103 PUBLICATIONS **1,875** CITATIONS
SEE PROFILE

NANO LETTERS

2003
Vol. 3, No. 1
65−67

Dichroic Thin Films of Silver Nanoparticle Chain Arrays on Facetted Alumina Templates

E. Fort,* C. Ricolleau, and J. Sau-Pueyo

Pôle Matériaux et Phénomènes Quantiques, Fédération de Recherche CNRS 2437 (SPM) and Laboratoire de Minéralogie-Cristallographie de Paris, UMR CNRS 7590, Universités Paris VI et Paris VII, 4 place Jussieu, 75252 Paris Cedex, France

Received September 23, 2002; Revised Manuscript Received November 18, 2002

ABSTRACT

We show that controlled growth on ordered facetted alumina substrates can be used as nanoscale templates to produce regular arrays of silver nanoparticle chains. The interactions between the aligned nanoparticles induce strong dichroism in the absorption spectra. The resonance plasmon wavelengths are shifted to 455 and 550 nm for transverse and longitudinal polarization, respectively. Simulations show that the slightly prolate shape of the nanoparticles also contributes to the resonance splitting. Such nanostructured thin films can be used as dichroic devices.

The electronic confinement in silver nanoparticles induces dramatic changes in the optical properties. These changes are caused by surface plasmon resonances that come from the electromagnetic (EM) field excitation inside the particles associated with the collective oscillation of the electrons. Interactions between closely spaced metallic nanoparticles shift the frequency of the surface plasmon resonance through EM coupling.[1] These interactions induce different spectral responses depending on the light polarization in films with anisotropic local surroundings. Linear chains of silver nanoparticles can thus be used as dichroic devices.[2]

The collective properties of nanostructured thin films have also focused much attention in recent years on other potentially promising applications. In particular, linear chains of metallic nanoparticles can be used in waveguiding systems to overcome the size limits of conventional dielectric wave optics since they can transport EM energy below the diffraction limit.[3,4] Besides, these nanostructured materials could be used in optical transistors based on local field enhancement at the plasmon resonance[5] or spectrally coded optical memory devices.[6]

Step decoration on periodically stepped substrates has been used for many years to obtain arrays of nanowires taking advantage of the preferential nucleation sites on the step ledges for the metal adatoms due to the increased coordination with respect to the terrace sites.[7] In this letter, we show how controlled growth on ordered facetted alumina substrates can be used as nanoscale templates to produce ordered arrays of silver nanoparticle chains with dichroic optical properties. This technique potentially offers an elegant alternative to the electron-beam lithography technique.

Vicinal surfaces are obtained when the surface normal deviates slightly from that of the surface in the equilibrium form; surface faceting occurs when the angle between the original surface normal and that of the equilibrium form is large. This transformation of the initial surface into a "hill-and-valley" structure is commonly observed on many surfaces.[8]

The facetted alumina substrate is obtained from an optically polished Al_2O_3 single crystal with a nominal $(10\bar{1}0)$ orientation. The sample is cleaned in sulfuric acid, followed by rinsing in successive baths of distilled water and methanol before being dried with filter paper. The sample is then annealed in air for 8 h at 1400 °C. In the furnace, the sample is protected from contamination by being enclosed in a high-purity alumina protective shell.

Silver deposition is performed by a pulsed-laser deposition (PLD) technique using a silver target. The average deposition rate, measured by Rutherford backscattering spectrometry, is 3×10^{-3} nm s^{-1} for a pulse repetition rate of 2 Hz. The substrate is placed at 400 °C under a residual pressure of about 10^{-6} mbar. The protective deposition of an amorphous alumina coating is performed using an Al_2O_3 target under the same experimental conditions.

The transmission electron microscopy (TEM) images are obtained using a JEOL 2000 EX electron microscope operating at 200 kV. The image resolution is about 0.5 nm. Optical spectra are acquired using a Cary 500 Varian differential optical spectrometer. The field-emission gun scanning electron microscopy (SEMFEG) experiments are performed on a Leo Gemini operating at 2 keV.

* To whom correspondence should be addressed. E-mail: Emmanuel.Fort@lmcp.jussieu.fr.

10.1021/nl025808r CCC: $25.00
Published on Web 12/06/2002

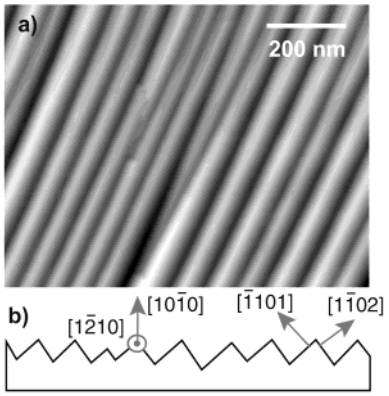

Figure 1. (a) AFM image of the facetted alumina surface after a heating treatment for 8 h at 1400 °C. (b) Schematic of the facetted profile with the associated crystallographic directions.

Figure 1 shows the AFM image of the facetted alumina surface together with a schematic profile of the "hill-and-valley" structure. The crystallographic directions and facet indexes are also indicated.

The crystallographic directions given in Figure 1b have been deduced from TEM and X-ray diffraction patterns. The facet edges are oriented along the [12$\bar{1}$0] crystallographic direction. The surface indexes associated with the two kinds of facets are (1$\bar{1}$02) and ($\bar{1}$101). These experimental results agree with the results in ref 8.

The facetting process of the nominal (10$\bar{1}$0) alumina suface has been studied by J. R. Heffelfinger et al.[8,9] They show that the facetting process starts with the nucleation and growth of individual facets, which promote the subsequent nucleation of other adjacent facets, thus forming facetted domains. These domains grow and ultimately coalesce. However, since they are not in phase, facet junctions appear. Facet coarsening takes place through junction motion and elimination.

The facet width is determined by two successive mechanisms. The facet width reaches its first critical value as it widens during the start of the facetting process until it induces adjacent facet formation. The second mechanism is due to surface coarsening through junction elimination. In our case, the average width reached after annealing for 8 h at 1400 °C is about 50 nm and remains nearly constant for longer annealing times. Besides, the number of remaining junctions significantly depends on one particular sample for identical experimental annealing procedures. Their elimination is presumably limited by the initial misorientation of the surface since a certain density of junctions is probably needed to maintain the net orientation of the original surface after facetting.[8]

Figure 2 shows the SEM image of the facetted alumina surface as it appears before (left) and after (right) silver deposition at 400 °C. It also shows a schematic of the covered surface profile (Figure 2b). The uncoated part of the surface is obtained after gently scratching the surface to remove the silver nanoparticles. From a simple inspection of the image, it is clearly visible that silver grows in nanoparticles, forming a regular array of nanochains along the "hill-and-valley"

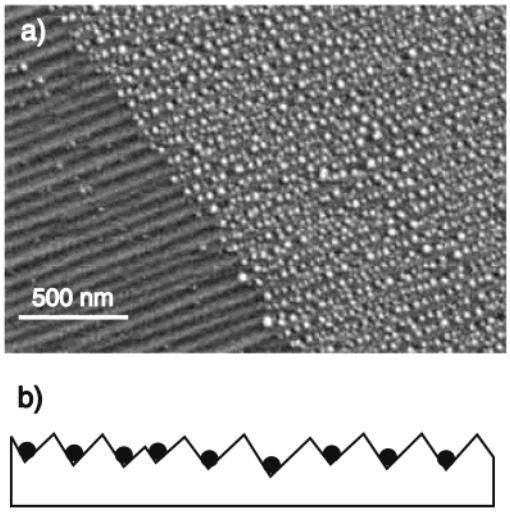

Figure 2. (a) SEM image of the facetted alumina surface as it appears before (left) and after (right) silver deposition at 400 °C by PLD. (b) Schematic of the surface profile after silver nanoparticle deposition.

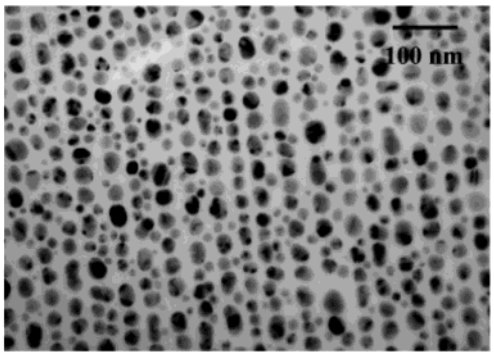

Figure 3. TEM image of the facetted alumina surface covered with chains of silver nanoparticles.

profiles. The nanoparticles are situated in the grooves, the spacing between two adjacent chains being equal to the facet wavelength. These positions are not surprising since the grooves are preferential nucleation sites because of their increased coordination number with respect to that of the terrace sites. The ridges act as barriers preventing the silver adatoms from diffusing across two adjacent facets. At 400 °C, the silver atoms do not have enough thermal energy to overcome the edge barrier.

Figure 3 shows the TEM image of the silver nanoparticles deposited on the facetted alumina substrate. The high resolution and large magnification ($\times$100 000) of the TEM image allows us to retrieve details on a single chain structure. The chains consist of nearly spherical silver nanoparticles with an average transverse size of about 25 nm and an average spacing from center to center of about 31 nm. The particles have a slightly prolate shape along the chain axis: their longitudinal size a is about 27 nm. To avoid nucleation on the terraces, it is necessary to perform the growing process at sufficiently high temperature. The mean free path of a silver adatom must be large compared to the facet width to reach the groove to nucleate. The temperature is, however, limited to avoid interfacet diffusion.

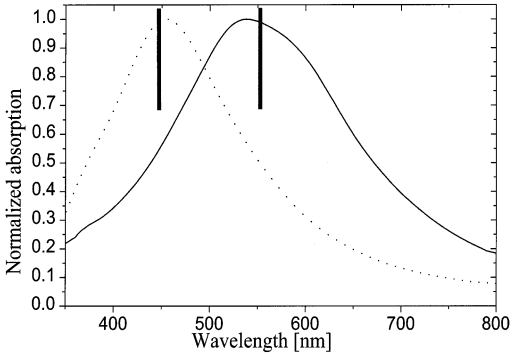

Figure 4. Normalized optical absorption spectra for longitudinal (—) and transverse (••) polarizations of the incident EM field. The vertical lines correspond to the resonance positions obtained by the model.

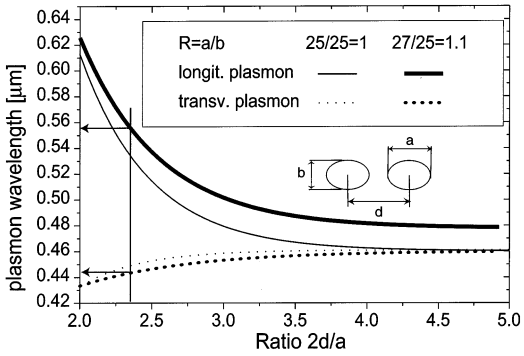

Figure 5. Evolution of the surface plasmon wavelength vs interparticle spacing for particles with spheroid and prolate ellipsoid ($R = 1.1$) shapes. The distance between two adjacent lines is 50 nm. The arrows correspond to the experimental configuration.

Figure 4 shows the optical spectra obtained for light polarization parallel (solid line) and perpendicular (dotted line) to the particle chains. The surface plasmon resonance is clearly visible on both spectra. This resonance is centered around 455 and 550 nm for the parallel and perpendicular polarizations, respectively. The fwhm of the transverse resonance is about 100 nm whereas the one associated with the longitudinal plasmon is about 200 nm.

To analyze the absorption spectra, we use the model developed by Yamagushi et al., which is a continuation of the Maxwell−Garnett theory. The shape of the particles and the interparticle interaction are taken into account.[1] Since the particles' dimensions are much smaller than the wavelength of light, we consider the so-called quasistatic approximation. The particles are modelized as polarizable ellipsoids with their principal axis a oriented along the chain direction x. The polarizability α_i along one of the axis directions is

$$\alpha_i = V \frac{\epsilon_1 - \epsilon_m}{\epsilon_m + L_i(\epsilon_1 - \epsilon_m)} \text{ for } i = x \text{ or } y \qquad (1)$$

where V is the ellipsoid volume and L_i is a shape factor that depends on the axial ratio $R = a/b$ of the particle[2]; ϵ_1 and ϵ_m are the dielectric constants of the substrate and the metal, respectively.

The local field E_{loc} for a given particle is the sum of the incident field E_0 and the fields scattered by the surrounding particles. The local field can be written as

$$E_{loc} = E_0/(1 + \alpha\beta) \qquad (2)$$

where β represents the interaction constant that depends on a particular geometry. β is real if the field retardation effects are neglected.

Figure 5 shows the influence of the particle interaction on the plasmon resonance position for different particle shapes $R = 1$ (spheroid) and 1.1 (prolate ellipsoid). The solid lines represent the polarization along the chains, and the dotted lines represent the orthogonal polarization. The distance between two adjacent chains is 50 nm. For spheroid particles, the influence of the interaction between the nanoparticles is clearly visible. The longitudinal plasmon shifts toward the red by about 80 nm for touching particles whereas the transverse plasmon is blue-shifted by 20 nm. As the distance between two adjacent particles is increased, the splitting decreases to reach zero for square geometry. The prolate shape of the particles adds an additional splitting that is nearly independent of the particles' spacing: for $R = 1.1$, the additional splitting is about 20 nm. Both effects contribute to the dichroism of the thin film. The positions of the plasmon resonances deduced from the model are in good agreement with the experimental ones (see vertical lines in Figure 4).

In summary, we have shown that it is possible to use facetted alumina surfaces to produce well-organized chains of silver nanoparticles. These materials possess strong optical dichroism that is readily applicable to ultrathin dichroic devices. Besides, other important applications are also promising, taking advantage of the local field enhancement.[5,6]

Acknowledgment. We acknowledge C. Belouet for fruitful discussions. This work is supported by Alcatel as part of the DEMETER program.

References

(1) Yamagushi, T.; Yoshida, S.; Kinbara, A. *Thin Solid Films* **1974**, *21*, 173.
(2) Gotschy, W.; Vonmetz, K.; Leitner, A.; Aussenegg, F. R. *Opt. Lett.* **1996**, *21*, 1099.
(3) Takahara, J.; Yamagushi, S.; Taki, H.; Morimoto, A.; Kobayashi, T. *Opt. Lett.* **1997**, *22*, 475.
(4) Quinten, M.; Leitner, A.; Krenn, J. R.; Aussenegg, F. R. *Opt. Lett.* **1998**, *23*, 1331.
(5) Tominaga, J.; Mihalcea, C.; Büchel, D.; Fukuda, H.; Nakano, T.; Atoda, N.; Fuji, H.; Kikukawa, T. *Appl. Phys. Lett.* **2001**, *78*, 2417.
(6) Ditlbacher, H.; Krenn, J. R.; Lamprecht, B.; Leitner, A.; Aussenegg, F. R. *Opt. Lett.* **2000**, *25*, 563.
(7) Gambardella, P.; Blanc, M.; Brune, H.; Kuhnke, K.; Kern, K. *Phys. Rev. B* **2000**, *61*, 2254.
(8) Heffelfinger, J. R.; Barry Carter, C. *Surf. Sci.* **1997**, *389* 188.
(9) Heffelfinger, J. R.; Bench, M. W.; Barry Carter, C. *Surf. Sci. Lett.* **1995**, *343*, L1161.

NL025808R